8376 *Inorg. Chem.* **2009**, *48*, 8376–8382
DOI: 10.1021/ic901064q

Inorganic Chemistry
Article

New Noncentrosymmetric Material - $[N(CH_3)_4]ZnCl_3$: Polar Chains of Aligned $ZnCl_4$ Tetrahedra

Myung-Ho Choi,[†] Sang-Hwan Kim,[‡] Hong-Young Chang,[‡] P. Shiv Halasyamani,[‡] and Kang Min Ok*,[†]

[†]*Department of Chemistry, Chung-Ang University, 221 Heukseok-dong, Dongjak-gu, Seoul 156-756, Republic of Korea, and* [‡]*Department of Chemistry, University of Houston, 136 Fleming Building, Houston, Texas 77204-5003*

Received June 3, 2009

A new organically templated noncentrosymmetric polar zinc chloride, $[N(CH_3)_4]ZnCl_3$, has been synthesized hydrothermally, and the structure was determined by single crystal X-ray diffraction. The reported material exhibits a unidimensional crystal structure consisting of chains of anionic $ZnCl_4$ tetrahedra that are separated by $[N(CH_3)_4]^+$ cations. Second-harmonic generation (SHG) measurement on the noncentrosymmetric $[N(CH_3)_4]ZnCl_3$, using 1064 nm radiation, indicate the material has a SHG efficiency of approximately $15 \times \alpha$-SiO_2. Additional SHG measurements indicate the material is nonphase-matchable (type 1). In addition, converse piezoelectric measurements revealed d_{33} values of 10 pm/V. Thermogravimetric analysis, UV−vis diffuse reflectance, and infrared spectroscopy were also performed, as were electronic structure calculations. Crystal data: $[N(CH_3)_4]ZnCl_3$, orthorhombic, space group $Pmc2_1$ (No. 26), with a = 7.2350(14) Å, b = 8.8210(18) Å, c = 15.303(3) Å, V = 976.6(3) Å^3, and Z = 4.

Introduction

Noncentrosymmetric (NCS) materials containing asymmetric coordination environments are of significant and broad interest attributed to various technologically important functional properties such as second harmonic generation (SHG), piezoelectricity, ferroelectricity, and pyroelectricity.[1−5] Whether the materials have molecular or extended solid-state structures, a number of strategies have been suggested to increase the incidence of crystallographic NCS in any new material.[6−11] The rational synthesis of crystallographically NCS materials, however, remains an ongoing challenge. With oxide materials, cations susceptible to second-order Jahn−Teller (SOJT) distortions, that is, octahedrally coordinated d^0 transition-metal ions (Ti^{4+}, V^{5+}, Mo^{6+}, etc.) and lone-pair cations (Pb^{2+}, Sb^{3+}, Te^{4+}, I^{5+}, etc.), have been shown to produce NCS structures with their inherent asymmetric coordination environments.[12−23] For the d^0 metal ions, an out-of-center displacement toward a corner, edge, or face of the octahedron attributable to mixing between the empty metal d- and filled oxygen p-orbitals is responsible for the asymmetric geometry;[24] whereas, with the lone-pair cations, a nonbonded

*To whom correspondence should be addressed. E-mail: kmok@cau.ac.kr. Phone: +82-2-820-5197. Fax: +82-2-825-4736.

(1) Jona, F.; Shirane, G., *Ferroelectric Crystals*; Pergamon Press: Oxford, U.K., 1962.
(2) Cady, W. G. *Piezoelectricity; an Introduction to the Theory and Applications of Electromechanical Phenomena in Crystals*; Dover: New York, 1964.
(3) Lang, S. B. *Sourcebook of Pyroelectricity*; Gordon & Breach Science: London, 1974.
(4) Galy, J.; Meunier, G. *J. Solid State Chem.* **1975**, *13*, 142.
(5) Lines, M. E.; Glass, A. M. *Principles and Applications of Ferroelectrics and Related Materials*; Oxford University Press: Oxford, U.K., 1991.
(6) Bruce, D.; Wilkinson, A. P.; While, M. G.; Bertrand, J. A. *J. Solid State Chem.* **1996**, *125*, 228.
(7) Kepert, C. J.; Prior, T. J.; Rosseinsky, M. J. *J. Am. Chem. Soc.* **2000**, *122*, 5158.
(8) Maggard, P. A.; Stern, C. L.; Poeppelmeier, K. R. *J. Am. Chem. Soc.* **2001**, *123*, 7742.
(9) Evans, O. R.; Lin, W. *Acc. Chem. Res.* **2002**, *35*, 511.
(10) Hwu, S.-J.; Ulutagay-Kartin, M.; Clayhold, J. A.; Mackay, R.; Wardojo, T. A.; O'Connor, C. J.; Kraweic, M. *J. Am. Chem. Soc.* **2002**, *124*, 12404.
(11) Welk, M. E.; Norquist, A. J.; Arnold, F. P.; Stern, C. L.; Poeppelmeier, K. R. *Inorg. Chem.* **2002**, *41*, 5119.
(12) Halasyamani, P. S.; Poeppelmeier, K. R. *Chem. Mater.* **1998**, *10*, 2753.
(13) Ok, K. M.; Bhuvanesh, N. S. P.; Halasyamani, P. S. *Inorg. Chem.* **2001**, *40*, 1978.
(14) Ok, K. M.; Bhuvanesh, N. S. P.; Halasyamani, P. S. *J. Solid State Chem.* **2001**, *161*, 57.
(15) Goodey, J.; Broussard, J.; Halasyamani, P. S. *Chem. Mater.* **2002**, *14*, 3174.
(16) Goodey, J.; Ok, K. M.; Broussard, J.; Hofmann, C.; Escobedo, F. V.; Halasyamani, P. S. *J. Solid State Chem.* **2003**, *175*, 3.
(17) Ra, H.-S.; Ok, K. M.; Halasyamani, P. S. *J. Am .Chem. Soc.* **2003**, *125*, 7764.
(18) Ok, K. M.; Halasyamani, P. S. *Angew. Chem., Int. Ed.* **2004**, *43*, 5489.
(19) Ok, K. M.; Halasyamani, P. S. *Inorg. Chem.* **2005**, *44*, 9353.
(20) Chi, E. O.; Ok, K. M.; Porter, Y.; Halasyamani, P. S. *Chem. Mater.* **2006**, *18*, 2070.
(21) Sivakumar, T.; Chang, H. Y.; Baek, J.; Halasyamani, P. S. *Chem. Mater.* **2007**, *19*, 4710.
(22) Chang, H. Y.; Sivakumar, T.; Ok, K. M.; Halasyamani, P. S. *Inorg. Chem.* **2008**, *47*, 8511.
(23) Chang, H. Y.; Kim, S.-H.; Ok, K. M.; Halasyamani, P. S. *Chem. Mater.* **2009**, *21*, 1654.
(24) Goodenough, J. B. *Annu. Rev. Mater. Sci.* **1998**, *28*, 1.

 Published on Web 08/05/2009

electron pair is found.[25−27] Understanding the structural basis of the local asymmetric environments is extremely important, as these environments are one of the dominant factors that influence the materials' NCS properties. The local acentric environment is, however, a necessary, but not sufficient condition for generating macroscopic NCS: the material may crystallize in centrosymmetric structure with the acentric units aligned in an antiparallel manner. Thus, understanding the factors that determine *macroscopic* centricity is equally as important as understanding the local asymmetry. Recently, we have demonstrated that macroscopic polarity can be controlled by the alkali metal cations in the $A_2Ti(IO_3)_6$ (A = Li, Na, K, Rb, Cs, Tl) system using cation size arguments, coordination preferences, and bond valence concepts.[28] Poeppelmeier et al. also reported that changes to the bond network, that is, the interactions between the asymmetric polyhedra and the framework cations can lead to different crystal symmetries, polar or nonpolar, with transition-metal oxyfluorides $[MO_xF_{6-x}]^{n-}$ (M = d^0 transition metal, x = 1−3, and n = 2, 3).[8,11,29−31] In this paper, we report on the synthesis and characterization of a new organically templated zinc chloride, $[N(CH_3)_4]ZnCl_3$. Although a number of zinc chloride materials such as $ZnCl_2$,[32] A_2ZnCl_4 (A = Li, Na, K, Rb, Cs, NH_4, $N(CH_3)_4$, $C(NH_2)_3$),[33−42] and $BaZnCl_4$,[43,44] have been reported, to the best of our knowledge, $[N(CH_3)_4]ZnCl_3$ is the first material exhibiting asymmetric alignment of the $ZnCl_4$ tetrahedra with a chain structure. Thus, we are going to explore the influence of the asymmetric alignment of the $ZnCl_4$ tetrahedra on the materials' properties. As such, second-harmonic generation, piezoelectricity, thermogravimetric, infrared, and UV−vis measurements, and electronic structure calculations on $[N(CH_3)_4]ZnCl_3$ were performed. We also describe structure−property relationships on the basis of all these experiments and calculations.

Experimental Section

Reagents. Tetramethylammonium chloride (Aldrich, 97%) and ZnO (Waco, 99.0) were used as received.

Table 1. Crystallographic Data for $[N(CH_3)_4]ZnCl_3$

formula	$[N(CH_3)_4]ZnCl_3$
f. w.	245.87
space group	$Pmc2_1$ (No. 26)
a (Å)	7.2350(14)
b (Å)	8.8210(18)
c (Å)	15.303(3)
V (Å^3)	976.6(3)
Z	4
T (°K)	173.0(2)
λ (Å)	0.71073
ρ_{calcd} (g cm^{-3})	1.672
μ (mm^{-1})	3.263
$R(F)^a$	0.0277
$R_w(F_o^2)^b$	0.0523

$^a R(F) = \sum||F_o| - |F_c||/\sum|F_o|$. $^b R_w(F_o^2) = [\sum w(F_o^2 - F_c^2)^2/\sum w(F_o^2)^2]^{1/2}$.

Table 2. Selected Bond Distances (Å) for $[N(CH_3)_4]ZnCl_3$

Zn(1)−Cl(1) × 2	2.3578(14)	N(1)−C(1)	1.483(11)
Zn(1)−Cl(2)	2.223(2)	N(1)−C(2)	1.513(10)
Zn(1)−Cl(3)	2.206(2)	N(1)−C(3) × 2	1.493(6)
Zn(2)−Cl(1) × 2	2.3516(14)	N(2)−C(4)	1.455(12)
Zn(2)−Cl(4)	2.236(2)	N(2)−C(5)	1.470(11)
Zn(2)−Cl(5)	2.200(2)	N(2)−C(6) × 2	1.483(8)

Synthesis. A 0.424 g (3.88×10^{-3} mol) portion of $[N(CH_3)_4]$-Cl, 0.316 g (3.88×10^{-3} mol) of ZnO, and 2.0 mL of HCl (aq. 35 wt %) were combined with 1.0 mL of H_2O. The reaction mixture was placed in a 23 mL Teflon-lined autoclave that was subsequently sealed. The autoclave was gradually heated to 150 °C, held for 12 h, and cooled slowly to room temperature at a rate of 6 °C h^{-1}. The product was recovered by filtration and dried in vacuum. Pure colorless crystals, the only product from the reaction, of $[N(CH_3)_4]ZnCl_3$ were obtained in 78% yield based on the ZnO.

Single Crystal X-ray Diffraction. A colorless rod (0.03×0.05×0.13 mm^3) was used for single crystal data analysis. All of the data were collected using a Bruker SMART APEX diffractometer equipped with a 1K CCD area detector using graphite monochromated Mo Kα radiation at 173 K at the Korea Basic Science Institute. A hemisphere of data was collected using a narrow-frame method with scan widths of 0.30° in ω, and an exposure time of 5 s/frame. The first 50 frames were remeasured at the end of the data collection to monitor instrument and crystal stability. The maximum correction applied to the intensities was <1%. The data were integrated using the SAINT program,[45] with the intensities corrected for Lorentz, polarization, air absorption, and absorption attributable to the variation in the path length through the detector faceplate. A semiempirical absorption correction was made on the hemisphere of data with the SADABS program.[46] The data were solved and refined using SHELXS-97 and SHELXL-97, respectively.[47,48] All of the atoms were refined with anisotropic thermal parameters and converged for $I > 2\sigma(I)$. All calculations were performed using the WinGX-98 crystallographic software package.[49] Crystallographic data and selected bond distances for the reported material are given in Tables 1 and 2.

Powder X-ray Diffraction. Powder X-ray diffraction was used to confirm the phase purity for each sample. The X-ray powder diffraction data were collected on a Scintag XDS2000 diffractometer at room temperature (Cu Kα radiation, $\theta-\theta$ mode, flat

(25) Gillespie, R. J.; Nyholm, R. S. *Q. Rev., Chem. Soc.* **1957**, *11*, 339.
(26) Orgel, L. E. *J. Chem. Soc.* **1959**, 3815.
(27) Seshadri, R.; Hill, N. A. *Chem. Mater.* **2001**, *13*, 2892.
(28) Chang, H. Y.; Kim, S.-H.; Ok, K. M.; Halasyamani, P. S. *J. Am . Chem. Soc.* **2009**, *131*, 6865.
(29) Maggard, P. A.; Nault, T. S.; Stern, C. L.; Poeppelmeier, K. R. *J. Solid State Chem.* **2003**, *175*, 27.
(30) Izumi, H. K.; Kirsch, J. E.; Stern, C. L.; Poeppelmeier, K. R. *Inorg. Chem.* **2005**, *44*, 884.
(31) Marvel, M. R.; Lesage, J.; Baek, J.; Halasyamani, P. S.; Stern, C. L.; Poeppelmeier, K. R. *J. Am. Chem. Soc.* **2007**, *129*, 13963.
(32) Brynestad, J.; Yakel, H. L. J. *Inorg. Chem.* **1978**, *17*, 1376.
(33) McGinnety, J. A. *Inorg. Chem.* **1974**, *13*, 1057.
(34) Matsunaga, H. *J. Phy. Soc. Jpn.* **1982**, *51*, 864.
(35) Matsunaga, H.; Itoh, K.; Nakamura, E. *Acta Crystallogr.* **1982**, *B38*, 898.
(36) van Koningsveld, H. *Acta Crystallogr.* **1983**, *C39*, 15.
(37) Madariaga, G.; Zuniga, F. J.; Perez-Mato, J. M.; Tello, M. J. *Acta Crystallogr.* **1987**, *B43*, 356.
(38) Zhang, Z.; Lutz, H. D. *Z. Kristallogr.* **1995**, *210*, 691.
(39) Sassmannshausen, M.; Solinas, I.; Lutz, H. D. *Z. Kristallogr.* **1996**, *211*, 819.
(40) Furukawa, Y.; Ishida, H.; Kashino, S. *Z. Kristallogr. - New Cryst. Struct.* **1999**, *214*, 367.
(41) Ferrari, E. S.; Roberts, K. J.; Thomson, G. B.; Gale, J. D.; Catlow, C. R. A. *Acta Crystallogr.* **2001**, *A57*, 264.
(42) Aramburu, I.; Friese, K.; Perez-Mato, J. M.; Morgenroth, W.; Aroyo, M.; Breczewski, T.; Madariaga, G. *Phy. Rev. B: Condens. Matter* **2006**, *73*, 014112–1.
(43) Wickleder, C.; Masselmann, S.; Meyer, G. *Z. Anorg. Allg. Chem.* **1999**, *625*, 507.
(44) Wickleder, C. *J. Solid State Chem.* **2001**, *162*, 237.
(45) *SAINT, Program for Area Detector Absorption Correction*, Version 4.05; Siemens Analytical X-ray Instruments: Madison, WI, 1995.
(46) Blessing, R. H. *Acta Crystallogr.* **1995**, *A51*, 33.
(47) Sheldrick, G. M. *SHELXS-97 - A program for automatic solution of crystal structures*; University of Goettingen: Goettingen, Germany, 1997.
(48) Sheldrick, G. M. *SHELXL-97 - A program for crystal structure refinement*; University of Goettingen: Goettingen, Germany, 1997.
(49) Farrugia, L. J. *J. Appl. Crystallogr.* **1999**, *32*, 837.

plate geometry) equipped with Peltier germanium solid state detector in the 2θ range 5−70° with a step size of 0.02°, and a step time of 1 s. The experimental powder XRD pattern is in good agreement with the calculated data from the single-crystal model.

Elemental Analysis. Elemental analysis was carried out by a Carlo Erba EA1108 analyzer. Elemental microanalysis for $[N(CH_3)_4]ZnCl_3$ obsd (calcd): C, 19.54% (19.51%); H, 4.92% (4.81%); N, 5.70% (5.61%).

Infrared Spectroscopy. Infrared spectrum was recorded on a Varian 1000 FT-IR spectrometer in the 400−4000 cm^{-1} range, with the sample pressed between two KBr pellets.

UV−vis Diffuse Reflectance Spectroscopy. UV−visible reflectance data were collected on a Varian Cary 500 scan UV−vis-NIR spectrophotometer over the spectral range 200−1500 nm at room temperature. Poly(tetrafluoroethylene) was used as a reference material. The reflectance spectrum was converted to the absorbance using the Kubelka−Munk function.[50,51]

Thermogravimetric Analysis (TGA). TGA was performed on a Setaram LABSYS TG-DTA/DSC Thermogravimetric Analyzer. The polycrystalline $[N(CH_3)_4]ZnCl_3$ sample was contained within a platinum crucible and heated at a rate of 10 °C min^{-1} from room temperature to 800 °C under flowing argon.

Second-Order Nonlinear Optical Measurements. Powder SHG measurements on polycrystalline $[N(CH_3)_4]ZnCl_3$ were performed on a modified Kurtz-NLO system[52] using 1064 nm radiation. A detailed description of the equipment and the methodology used has been published.[53] SHG efficiency has been shown to depend strongly on particle size, thus polycrystalline samples were ground and sieved into distinct particle size ranges (20−45, 45−63, 63−75, 75−90, >90 μm). To make relevant comparisons with known SHG materials, crystalline α-SiO_2 and $LiNbO_3$ were also ground and sieved into the same particle size ranges. Powders with particle size 45−63 μm were used for comparing SHG intensities. No index matching fluid was used in any of the experiments.

Piezoelectric Measurements. Piezoelectric measurements were performed using a Radiant Technologies RT66A piezoelectric test system with a TREK (model 609E−6) high voltage amplifier, Precision Materials Analyzer, Precision High Voltage Interface, and MTI 2000 Fotonic Sensor. The polycrystalline $[N(CH_3)_4]ZnCl_3$ was pressed into a 12 mm diameter and ~0.8 mm thick pellet. The pellet was annealed at 200 °C for 6 h. A conducting silver paste was applied to both sides of the pellet surfaces for electrodes. A maximum voltage of 500 V was applied to the sample.

Electronic Structure Calculations. First principle electronic band structure for NCS polar $[N(CH_3)_4]ZnCl_3$ was carried out using plane wave pseudopotential calculations as implemented in the Quantum ESPRESSO (4.0.1 version) package.[54] Ultrasoft (US)[55] and norm-conserving Martins−Troullier (MT) pseudopotentials (PP)[56] were utilized with the generalized gradient approximation (GGA)[57] for the exchange-correlation corrections. A plane wave energy cutoff was set to 37 Ry. A total of k-point grid of $4 \times 4 \times 2$ was used for Brillouin zone integration. A total energy convergence threshold was set to 10^{-6} Rydberg.

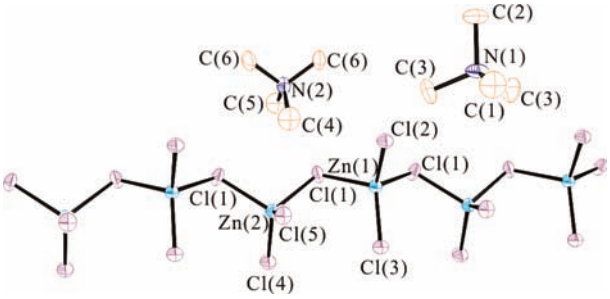

Figure 1. ORTEP (50% probability ellipsoids) drawing for $[N(CH_3)_4]ZnCl_3$. Hydrogen atoms have been removed for clarity.

Results and Discussion

Structure. $[N(CH_3)_4]ZnCl_3$ has a unidimensional crystal structure consisting of chains of $ZnCl_4$ tetrahedra that are separated by $[N(CH_3)_4]^+$ cations (see Figure 1). In connectivity terms, the structure may be written as infinite anionic chains of $[ZnCl_{2/2}Cl_{2/1}]^{1-}$ with charge balance maintained by the $[N(CH_3)_4]^+$ cations. Each of the two unique Zn^{2+} cations is linked to four chlorine atoms in a distorted tetrahedral environment with bond distances that range from 2.200(2) to 2.3578(14) Å. Two bridging zinc-chlorine bonds, Zn(1)−Cl(1) and Zn(2)−Cl(1), exhibit longer bond lengths of 2.3578(14) and 2.3516(14) Å, respectively. However, two terminal zinc-chlorine bonds show rather shorter bond distances (2.200(2)−2.236(2) Å). The Cl−Zn−Cl bond angles are in the range 98.70(7)−121.20(9)°. These bond distances and angles are consistent with those of previously reported zinc chlorides.[32−44] The two $ZnCl_4$ tetrahedra share their corners to form one-dimensional chains that run parallel to the a-axis (see Figure 2). Although there are slight deviations, interestingly, all the $ZnCl_4$ tetrahedra in the chains are approximately aligned in one direction (see Figure 3). As we will discuss in detail later, this alignment of the tetrahedra is responsible for the polar nature of $[N(CH_3)_4]ZnCl_3$ as well as its NCS properties. The organic template cation, $[N(CH_3)_4]^+$ resides within the crystal lattice and forms hydrogen bonds with the $ZnCl_4$ tetrahedra. The C−N bond lengths in $[N(CH_3)_4]^+$ range from 1.455(12) to 1.513(10) Å. The observed C−N−C bond angles range from 107.5(7) to 110.9(5)°. Crystallographically, $[N(CH_3)_4]ZnCl_3$ possesses a mirror plane perpendicular to the a-axis, a c-glide along the b-axis, and a 2_1 screw axis along the c-direction, resulting in the polar space group, $Pmc2_1$. Bond valence calculations[58,59] resulted in values of 2.02 and 2.03 for the two unique Zn^{2+} cations.

Infrared Spectroscopy. The infrared spectrum of $[N(CH_3)_4]ZnCl_3$ revealed C−H vibrations in the region of about 3000 and 1290−1490 cm^{-1}. Stretches centered at 914 and 948 cm^{-1} can be assigned to C−N vibrations. The infrared vibrations and assignments are listed in Table 3. The assignments are consistent with those previously reported.[60,61]

UV−vis Diffuse Reflectance Spectroscopy. UV−vis diffuse reflectance spectrum was collected on the reported $[N(CH_3)_4]ZnCl_3$ (see Figure S3 in the Supporting

(50) Kubelka, P.; Munk, F. *Z. Tech. Phys.* **1931**, *12*, 593.
(51) Tauc, J. *Mater. Res. Bull.* **1970**, *5*, 721.
(52) Kurtz, S. K.; Perry, T. T. *J. Appl. Phys.* **1968**, *39*, 3798.
(53) Ok, K. M.; Chi, E. O.; Halasyamani, P. S. *Chem. Soc. Rev.* **2006**, *35*, 710.
(54) Baroni, S.; Dal Corso, A.; de Gironcoli, S.; Giannozzi, P.; Cavazzoni, C.; Ballabio, G.; Scandolo, S.; Chiarotti, G.; Focher, P.; Pasquarello, A.; Laasonen, K.; Trave, A.; Car, R.; Marzari, N.; Kokalj, A., http://www.quantum-espresso.org/.
(55) Vanderbilt, D. *Phys. Rev. B* **1990**, *41*, 7892.
(56) Troullier, N.; Martins, J. L. *Phys. Rev. B* **1991**, *43*, 1993.
(57) Perdew, J. P.; Burke, K.; Ernzerhof, M. *Phys. Rev. Lett.* **1996**, *77*, 3865.
(58) Brown, I. D.; Altermatt, D. *Acta Crystallogr.* **1985**, *B41*, 244.
(59) Brese, N. E.; O'Keeffe, M. *Acta Crystallogr.* **1991**, *B47*, 192.
(60) Harmon, K. M.; Gennick, I.; Madeira, S. L. *J. Phy. Chem.* **1974**, *78*, 2585.
(61) Vico, S.; Palys, B.; Buess-Herman, C. *Langmuir* **2003**, *19*, 3282.

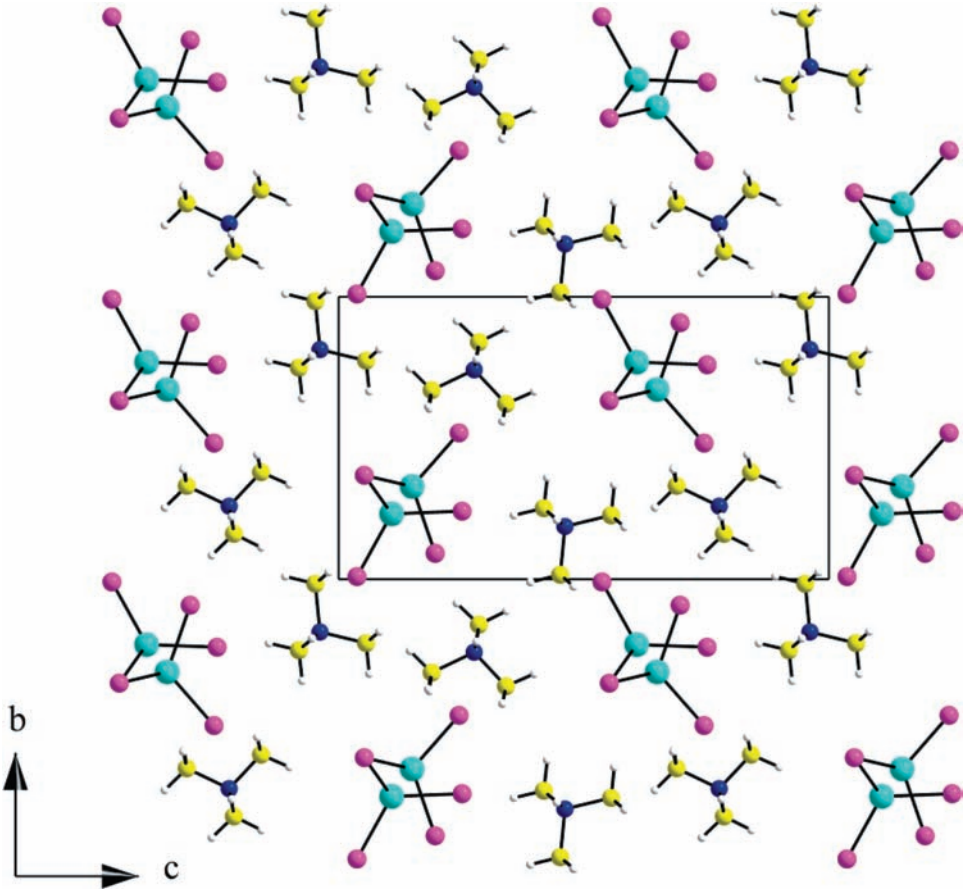

Figure 2. Ball-and-stick diagram of $[N(CH_3)_4]ZnCl_3$ in the *bc*-plane (cyan, Zn; purple, Cl; blue, N; yellow, C; white, H).

Information). Absorption (K/S) data were calculated from the following Kubelka−Munk function:[50,51]

$$F(R) = \frac{(1-R)^2}{2R} = \frac{K}{S}$$

where R is the reflectance, K the absorption, and S the scattering. In the (K/S)-versus-E plot, extrapolating the linear part of the rising curve to zero provided the onset of absorption at ~3.4 eV for $[N(CH_3)_4]ZnCl_3$. The band gap is mainly attributable to the interaction of the Zn−Cl bonds, consistent with our first-principles calculations (see the Calculations section).

TGA. The thermal behavior of $[N(CH_3)_4]ZnCl_3$ was investigated using TGA. TGA measurement revealed that the reported material decomposed above 340 °C and kept loosing organic molecules and chlorides. Calcd (exptl): 55.43% (55.19%). Considering that the boiling point of $ZnCl_2$ is 732 °C,[62] the weight of decomposed material kept decreasing under the flowing argon. The TGA data are shown in Figure S4 in the Supporting Information.

Functional Properties: SHG and Piezoelectricity. As $[N(CH_3)_4]ZnCl_3$ is NCS, we investigated its SHG and piezoelectric properties. Powder SHG measurements, using 1064 nm radiation, indicated that $[N(CH_3)_4]ZnCl_3$ has a SHG efficiency of approximately 15 × α-SiO_2. The observation of relatively low SHG intensity is not surprising, since the material does not contain any d^0 transition metals or lone-pair cations. However, the SHG efficiency is on the same order of ZnO.[52] By sieving $[N(CH_3)_4]ZnCl_3$ into various particle sizes, ranging from 20−150 μm, and measuring the SHG as a function of particle size, we were able to determine the type 1 phase-matching capabilities of the material. We determined that $[N(CH_3)_4]ZnCl_3$ is not phase-matchable (see Supporting Information). As previously shown, once the SHG efficiency has been measured and the phase-matching behavior determined, the average NLO susceptibility, $\langle d_{eff}\rangle_{exp}$, can be estimated.[15] For $[N(CH_3)_4]ZnCl_3$, $\langle d_{eff}\rangle_{exp}$ is approximately 2.1 pm/V. Converse piezoelectric measurements were performed on $[N(CH_3)_4]ZnCl_3$. Briefly, with the converse piezoelectric measurement a voltage is applied to the sample that produces a macroscopic deformation. A maximum voltage of 500 V was applied to the sample. Twenty measurements were performed, and an average was taken. The graph of the piezoelectric data has been deposited in the Supporting Information. The piezoelectric charge constant, d_{33}, was calculated from

$$\Delta L = S \times L_0 \sim E \times d_{33} \times L_0$$

where ΔL is the displacement of the sample, L_0 is the sample thickness (m), S is the strain ($\Delta L/L_0$), and E is the electric field strength (V/m). We estimate d_{33} values of 10 pm/V for $[N(CH_3)_4]ZnCl_3$. The value is similar to that of ZnO (d_{33} = 10.6−12.0 pm/V).[63]

(62) Lide, D. R. *CRC Handbook of Chemistry and Physics*; CRC Press: Boca Raton, FL, 2004.

(63) Landolt, H. *Numerical Values and Functions from the Natural Sciences and Technology* (*New Series*), *Group 3: Crystal and Solid State Physics*; Springer Verlag: Berlin, 1979; Vol. *11*, p 317 ff.

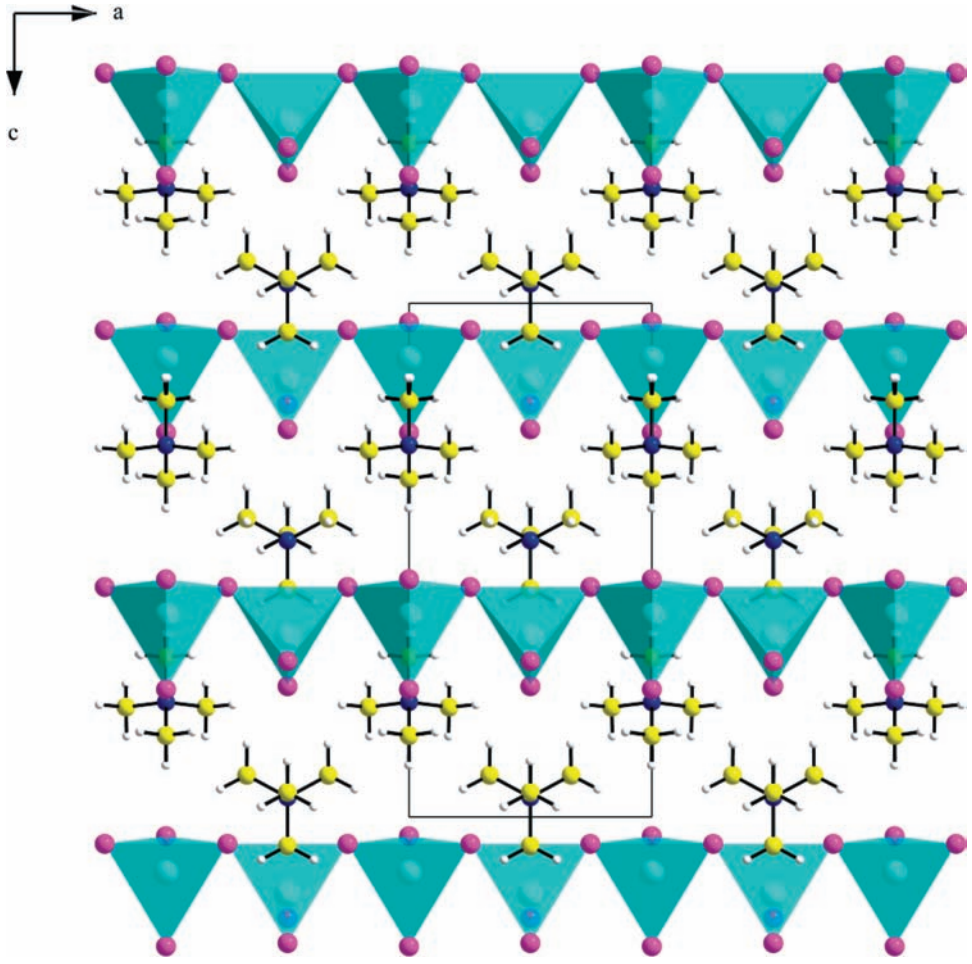

Figure 3. Ball-and-stick and polyhedral representation of $[N(CH_3)_4]ZnCl_3$ in the *ac*-plane (cyan, Zn; purple, Cl; blue, N; yellow, C; white, H). The $ZnCl_4$ tetrahedra share their corners to form one-dimensional chains along the [100] direction. Note all the $ZnCl_4$ tetrahedra are aligned in approximately the *c*-direction.

Table 3. Infrared Vibrations (cm^{-1}) for $[N(CH_3)_4]ZnCl_3$

ν(C−H)	δ(C−H)	ν(C−N)
3030	1483	948
2955	1448	914
2924	1418	
1295		

Calculations. The first principles density functional electronic band structure of $[N(CH_3)_4]ZnCl_3$ was calculated using the pseudopotential method. The electronic structure (see Figure 5) reveals an energy gap of ~3.6 eV appearing at the Fermi level (E_F). Although the calculated energy gap is slightly overestimated, it is qualitatively consistent with the experimentally observed value (~3.4 eV) in the UV−vis diffuse reflectance spectrum. To examine the detailed electronic structure, the total and projected density of states (DOSs) analyses were carried out. Several narrow valence bands exhibiting below ~ −3.8 eV are mainly composed of H, C, N, and Cl (3s) orbitals. A broad valence band exhibiting from −3.8 eV to E_F consists of larger contribution of Cl (3sp) orbitals and relatively small contribution of Zn (3d) orbitals. The conduction bands shown around ~4 eV are composed of equal contributions of Zn (4sp) and Cl (3sp) orbitals. Thus, it is indicative of the formation of the energy gap resulted from Zn−Cl bonds.

Structure−Property Relationships. As we described in the structure section, $[N(CH_3)_4]ZnCl_3$ crystallizes in the NCS polar space group $Pmc2_1$. A macroscopic polar environment is usually observed when locally polar asymmetric coordination polyhedra constructively add. For $[N(CH_3)_4]ZnCl_3$, the alignment of the $ZnCl_4$ tetrahedra in the chain and its NCS properties are mainly attributable to the polar crystal structure. The contribution of the organic template itself seems to be negligible in its property because the angles ∠C−N−C are very slightly off from those of the regular tetrahedron. Then, a question remains, what is the origin of the alignment of the $ZnCl_4$ tetrahedra? It has been known that the size of the cations plays a very important role in determining the centricity of the materials by affecting the interlayer spacing, the contact limits of other linkers, and the dimensions of the structure.[16,28] The hydrogen-bonding interaction is another crucial factor defining a unique polar axis in any polar structure.[64] For the reported material, the hydrogen-bonding between the hydrogens in the $[N(CH_3)_4]^+$ groups and the chlorines in the $ZnCl_4$ tetrahedra makes all the tetrahedra to point approximately in the [001] direction (see Figure 4). Thus, we analyzed the hydrogen bonds in

(64) Ok, K. M.; Baek, J.; Halasyamani, P. S.; O'Hare, D. *Inorg. Chem.* **2006**, *45*, 10207.

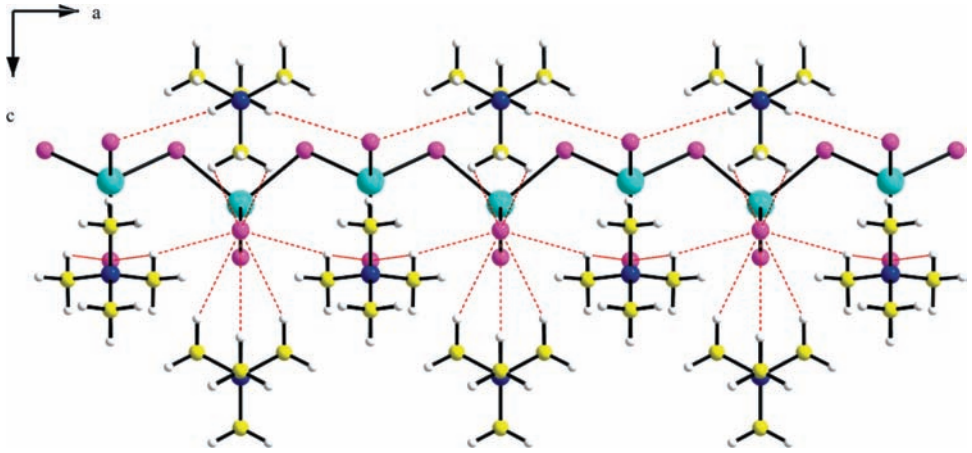

Figure 4. Ball-and-stick representation of $[N(CH_3)_4]ZnCl_3$ in the *ac*-plane to show the hydrogen-bondings between the hydrogens in the $[N(CH_3)_4]^+$ groups and the chlorines in the $ZnCl_4$ tetrahedra, which makes the $ZnCl_4$ tetrahedra aligned approximately in the *c*-direction (cyan, Zn; purple, Cl; blue, N; yellow, C; white, H).

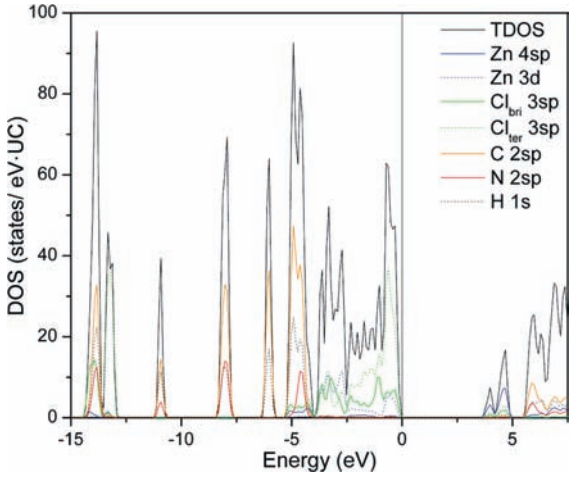

Figure 5. Total and projected density of states of $[N(CH_3)_4]ZnCl_3$. The vertical line at 0 eV indicates the Fermi level.

the structure and found that hydrogen bonds occur from C(1), C(2), C(3), and C(6) to the chlorine atoms in the $ZnCl_4$ tetrahedra [C(1)−H···Cl(3) 3.538(9) Å, C(2)−H···Cl(3) 3.963(9) Å, C(2)−H···Cl(4) 3.852(3) Å, C(3)−H···Cl(3) 3.871(6) Å, C(6)−H···Cl(3) 3.562(7) Å, C(6)−H···Cl(5) 3.772(7) Å; see Figure 4]. The observed hydrogen bonding interactions are consistent with those previously reported C−H···Cl distances.[65−67] Also, this similar distortion and/or alignment of tetrahedra attributable to the hydrogen-bonding were observed in the PO_3-(OH) tetrahedral environment.[64,68]

To better understand structure−property relationships as well as the asymmetric coordination environment of Zn^{2+}, we also calculated the local dipole moment for $[N(CH_3)_4]ZnCl_3$. This approach has been described earlier with respect to metal oxy-fluoride octahedra.[29,30] We recently reported the dipole moments for $BiCl_6$ octahedra as well.[69] Similarly, we found that the local dipole moments for the two unique $ZnCl_4$ tetrahedra, $Zn(1)Cl_4$ and $Zn(2)Cl_4$ are about 2.8 and 2.6 D (D = Debyes), respectively. For comparison, we have also calculated the local dipole moment for other known zinc chlorides (see Table 4). An examination of 27 examples of $ZnCl_4$ tetrahedra resulted in average dipole moments of 1.6 D. Although the difference is small, the local dipole moment values for $ZnCl_4$ tetrahedra in $[N(CH_3)_4]ZnCl_3$ are larger than others. We have also calculated the magnitude of the Zn^{2+} distortion in the

Table 4. Calculation of Dipole Moments for $ZnCl_4$ Tetrahedra

compound	species	dipole moment [D (Debyes)]
$ZnCl_2$[32]	$Zn(1)Cl_4$	0.31
Li_2ZnCl_4[39]	$Zn(1)Cl_4$	3.56
Na_2ZnCl_4[38]	$Zn(1)Cl_4$	2.75
K_2ZnCl_4[41]	$Zn(1)Cl_4$	1.94
K_2ZnCl_4[41]	$Zn(1)Cl_4$	1.89
	$Zn(2)Cl_4$	1.45
	$Zn(3)Cl_4$	2.00
Rb_2ZnCl_4[42]	$Zn(1)Cl_4$	1.55
Cs_2ZnCl_4[33]	$Zn(1)Cl_4$	1.21
$BaZnCl_4$[44]	$Zn(1)Cl_4$	2.70
$BaZnCl_4$[43]	$Zn(1)Cl_4$	0.67
$(NH_4)_2ZnCl_4$[36]	$Zn(1)Cl_4$	1.40
	$Zn(2)Cl_4$	1.28
	$Zn(3)Cl_4$	1.31
	$Zn(4)Cl_4$	1.37
	$Zn(5)Cl_4$	1.43
	$Zn(6)Cl_4$	1.15
	$Zn(7)Cl_4$	1.35
	$Zn(8)Cl_4$	1.26
$(NH_4)_2ZnCl_4$[35]	$Zn(1)Cl_4$	1.26
	$Zn(2)Cl_4$	1.64
	$Zn(3)Cl_4$	1.37
$(NH_4)_2ZnCl_4$[34]	$Zn(1)Cl_4$	1.37
$[N(CH_3)_4]_2ZnCl_4$[37]	$Zn(1)Cl_4$	0.28
$[C(NH_2)_3]_2ZnCl_4$[40]	$Zn(1)Cl_4$	1.40
$[N(CH_3)_4]ZnCl_3$[a]	$Zn(1)Cl_4$	2.78
	$Zn(2)Cl_4$	2.60
$ZnCl_4$ tetrahedra	(average)	1.60
27 examples[b]	(range)	0.28−3.56

[a] This work. [b] In the Supporting Information.

(65) Deshpande, M. S.; Kumbhar, A. S.; Puranik, V. G. *Cryst. Growth Des.* **2008**, *8*, 1952.
(66) Yoon, D.-W.; Gross, D. E.; Lynch, V. M.; Sessler, J. L.; Hay, B. P.; Lee, C.-H. *Angew. Chem., Int. Ed.* **2008**, *47*, 5038.
(67) Wu, J.-Y.; Hsu, H.-Y.; Chan, C.-C.; Wen, Y.-S.; Tsai, C.; Lu, K.-L. *Cryst. Growth Des.* **2009**, *9*, 258.
(68) Ok, K. M.; Doran, M. B.; O'Hare, D. *Dalton Trans.* **2007**, 3325.
(69) Kim, M. K.; Jo, V.; Kim, S. K.; Shim, I.-W.; Ok, K. M. *Bull. Korean Chem. Soc.* **2008**, *29*, 2273.

$ZnCl_4$ tetrahedra using continuous-symmetry measures.[70−73] For $[N(CH_3)_4]ZnCl_3$, the magnitudes are 0.046 and 0.040 $Å^2$ for Zn(1) and Zn(2), respectively. The distortion magnitudes are substantial for $ZnCl_4$ tetrahedra and consistent with the local dipole moment calculations. Also, one can find an effect of the size of alkali metal cations on the local dipole moments of $ZnCl_4$ tetrahedra in the orthorhombic A_2ZnCl_4 series. As the size of the alkali metal increases, the local dipole moment of $ZnCl_4$ tetrahedra decreases. As seen in Table 4, the average local dipole moments of $ZnCl_4$ tetrahedra for Li_2ZnCl_4, Na_2ZnCl_4, K_2ZnCl_4, Rb_2ZnCl_4, and Cs_2ZnCl_4 are 3.56, 2.75, 1.78, 1.55, and 1.21 D, respectively. In Li_2ZnCl_4 and Na_2ZnCl_4, the Li^+ and Na^+ cations are in pseudo-octahedral coordination environments. Thus, the Li^+ or Na^+ interact more strongly with chloride ligands on $ZnCl_4$ tetrahedra resulting in larger local dipole moments. However, the larger coordination environment of K^+, Rb^+, and Cs^+ makes rather weaker contacts to the chloride ligands, which results in relatively smaller local dipole moments for $ZnCl_4$ tetrahedra. While chains of $ZnCl_4$ tetrahedra can be easily formed in $[N(CH_3)_4]ZnCl_3$ attributable to the larger tetramethylammonium cation, isolated $ZnCl_4$ tetrahedra are normally observed in the compounds with smaller inorganic alkali metal cations. Instead, the larger dipole moments for $ZnCl_4$ tetrahedra in $[N(CH_3)_4]ZnCl_3$ seem to be attributable to the hydrogen bonding interactions. Furthermore, an examination of the chains in $[N(CH_3)_4]ZnCl_3$ using bond valence sums reveals large differences in the strengths of the Zn−Cl bonds. Bonds to terminal chlorines have valences ranging between 0.57 and 0.63, whereas the bonds to bridging chlorines show weaker valences (0.41−0.42). These differences may also be another source of the large dipole moments on the Zn centers in $[N(CH_3)_4]ZnCl_3$.

Acknowledgment. K.M.O and M.-H.C. thank the Nuclear Research & Development Program of National Research Foundation of Korea (NRF) funded by Ministry of Education, Science & Technology (MEST) (Grant 20090083266) for support. S.-H.K., H.-Y.C., and P.S.H. thank the Robert A. Welch Foundation (Grant E-1457), the ACS PRF 47345-AC10, and the NSF (DMR-0652150) for support.

Supporting Information Available: X-ray crystallographic file for $[N(CH_3)_4]ZnCl_3$ in CIF format, calculated and observed X-ray diffraction patterns, TGA diagram, phase-matching curve, displacement vs electric field loop for $[N(CH_3)_4]ZnCl_3$, and dipole moment calculations. This material is available free of charge via the Internet at http://pubs.acs.org.

(70) Zabrodsky, H.; Peleg, S.; Avnir, D. *J. Am. Chem. Soc.* **1992**, *114*, 7843.
(71) Alvarez, S.; Avnir, D.; Llunell, M.; Pinsky, M. *New J. Chem.* **2002**, *26*, 996.
(72) Llunell, M.; Casanova, D.; Cirera, J.; Bofill, J. M.; Alemany, P.; Alvarez, S.; Pinsky, M.; Avnir, D. *Shape Program*, version 1.1b; University of Barcelona: Barcelona, Spain, 2004.
(73) Alvarez, S.; Alemany, P.; Casanova, D.; Cirera, J.; Llunell, M.; Avnir, D. *Coord. Chem. Rev.* **2005**, *249*, 1693.